ISSN 0023-1584, Kinetics and Catalysis, 2024, Vol. 65, No. 5, pp. 586–596. © Pleiades Publishing, Ltd., 2024.

PHOTOCATALYSIS FOR ENERGY, ENVIRONMENTAL PROTECTION, AND SUSTAINABLE DEVELOPMENT

Reassembled Nanosheets of Layered Perovskite-Like Niobate $HCa_2Nb_3O_{10}$ as Photocatalysts for Hydrogen Production from Aqueous Solutions of Plant Biomass Processing Products

S. A. Kurnosenko[a], O. I. Silyukov[a], I. A. Rodionov[a], I. A. Minich[a], A. I. Ustinova[a], and I. A. Zvereva[a, *]

[a] *Institute of Chemistry, Saint Petersburg State University, St. Petersburg, 199034 Russia*

**e-mail: irina.zvereva@spbu.ru*

Received May 16, 2024; revised June 3, 2024; accepted June 11, 2024

Abstract—In conditions of depletion of mineral reserves, plant biomass is considered a renewable natural resource that can be photocatalytically processed to produce energy-intensive and environmentally friendly hydrogen fuel. In this regard, the present article focuses on the improvement of photocatalytic activity of the layered perovskite-structured niobate $HCa_2Nb_3O_{10}$ in the reactions of hydrogen production from aqueous solutions of typical plant biomass components, glucose and xylose, via its exfoliation into nanosheets followed by their reassembly and modification with a Pt cocatalyst. The reassembled compound obtained was shown to outperform in the activity the initial niobate and reference photocatalyst TiO_2 P25 Degussa up to 6.3 and 5.3 times, respectively, providing a hydrogen production rate up to 24.2 mmol $h^{-1}g^{-1}$ and apparent quantum efficiency up to 10% in the mid-near ultraviolet range.

Keywords: photocatalysis, hydrogen, plant biomass, perovskite nanosheets, exfoliation, reassembly

DOI: 10.1134/S0023158424601943

INTRODUCTION

In the context of continuously increasing anthropogenic pressure on the environment and depletion of mineral reserves, photocatalytic reforming of plant biomass components and derivatives represents a promising approach to producing hydrogen fuel that is characterized by an extremely high calorific value and the absence of secondary pollution in use [1–6]. Unlike natural gas and coal, traditionally serving as feedstock for hydrogen production, plant biomass is known to be a renewable resource, whose photocatalytic processing may be implemented using shareware solar radiation without releasing toxic substances into the environment. In addition, the use of plant biomass derivatives (bioalcohols, carbohydrates, carboxylic acids, etc.) [7–12] instead of pure water allows achieving much higher hydrogen production rates due to the absence of a kinetically hindered oxygen evolution half-reaction, which significantly limits the efficiency of water splitting [13–16].

In view of the above, an urgent task of modern chemical science is the design of new highly efficient photocatalysts for hydrogen production from plant biomass components. One of the most widely investigated materials to this day remains titanium dioxide TiO_2 [17–21], whose ability to split water into simple substances under ultraviolet irradiation was first demonstrated in the pioneering study of Japanese researchers Fujishima and Honda [22]. However, the performance of TiO_2-based photocatalysts often proves to be insufficient for practical use, which motivates scholars and engineers to explore other classes of photocatalytically active materials. One of the latter is represented by ion-exchangeable layered perovskite-like oxides—lamellar crystalline solids, whose structure consists of two-dimensional perovskite slabs, regularly interspersed with interlayer spaces occupied by cations [23]. Promising photocatalytic properties of these materials originate from the unique structure of the perovskite slabs, facilitating photogenerated charge carrier separation, and chemically active interlayer spaces capable of functioning as an additional reaction zone in photocatalytic processes [24]. Meanwhile, initial alkaline forms of most layered perovskite-like oxides are usually synthesized via the high-temperature ceramic technology that provides enhanced crystallinity of the corresponding photocatalysts at the expense of their specific surface area. One of the methods to overcome this problem consists in exfoliation of layered perovskite-structured materials into separate nanosheets [25, 26]. This, on the one hand, allows one to preserve practically significant properties of the perovskite matrix, and, on the other hand, to achieve a significant increase in the specific surface area. As a consequence, the resulting exfoliated materials possess a greater number of catalytically active sites and suffer less from volume electron-hole

recombination, which explains their improved photocatalytic performance [25].

The object of this study is the layered perovskite-like niobate $HCa_2Nb_3O_{10}$ that can be obtained via the substitution of interlayer alkali cations A' with protons in compounds $A'Ca_2Nb_3O_{10}$ [27]. The niobate in question represents one of the most well-known and well-proven perovskite-structured photocatalysts for hydrogen generation. Its nanosheets were revealed to exhibit hydrogen evolution activity in the aqueous solutions of methanol and isopropanol up to 9 mmol h^{-1} g^{-1} (500 W xenon lamp) [28] and 0.9 mmol h^{-1} g^{-1} (300 W xenon lamp) [29], respectively, as well as were used to yield composite photocatalysts with g-C_3N_4 [30], CdS [31, 32], Co_xP [33], Mo_2C [34], graphene oxide [35] and photosensitizing ruthenium complexes [36–38] to improve charge carrier separation and shift the long-wave absorption edge to the visible spectrum region. However, the issue of using perovskite-structured photocatalysts for reforming typical biomass-derived carbohydrates (for instance, glucose and xylose) still remains practically unaddressed although some of such materials were found to show a decent activity level in these reactions. Particularly, in accordance with one of our recent studies [39], the niobate $HCa_2Nb_3O_{10}$ after interlayer organic modification and surface decoration with a Pt cocatalyst can provide a hydrogen evolution rate (apparent quantum efficiency) in the aqueous solutions of glucose and xylose up to 18 mmol h^{-1} g^{-1} (7.5%) and 21 mmol h^{-1} g^{-1} (8.8%). The present article continues the aforementioned study and focuses on another approach to improving the niobate's activity in the reactions of glucose and xylose reforming—its exfoliation into nanosheets followed by their reassembly.

EXPERIMENTAL

Here and below, the protonated niobate $HCa_2Nb_3O_{10}$ and its reassembled form are abbreviated as HCN_3 and HCN_3 r/a, respectively.

Synthesis of HCN_3

The initial alkaline layered perovskite-like niobate $KCa_2Nb_3O_{10}$ was synthesized in accordance with the conventional ceramic method using pre-calcined Nb_2O_5, CaO and K_2CO_3 as reactants. The oxides were taken in stoichiometric amounts, the carbonate was weighed with a 30% excess compensating for the loss during calcination and providing formation of the target niobate in a single-phase state [40]. The reactants were mixed in a grinding bowl with silicon nitride balls and ground under an *n*-heptane layer in a Fritsch Pulverisette 7 (Germany) planetary micro mill at a rotation speed of 600 rpm, using a program of 10 repetitions of 10 min each separated by 5 min intervals. The mixture obtained was dried and pelletized into ~2 g tablets at a pressure of 50 bar using an Omec PI 88.00 (Italy) hydraulic press. Then, the tablets were placed into corundum crucibles with lids, calcined in a Nabertherm L-011K2RN (Germany) muffle furnace at 800°C for 12 h and at 1100°C for 24 h with intermediate grinding and repelletizing.

To obtain the protonated form of the niobate HCN_3, ground $KCa_2Nb_3O_{10}$ was treated with a 100-fold molar excess of 12 M nitric acid for 1 d under continuous stirring. After this, the product was centrifuged, thoroughly rinsed with water to remove acid residues and dried under ambient pressure. To avoid dehydration, HCN_3 was further stored in an atmosphere of humid air.

Exfoliation and Reassembly of HCN_3

The methodology for exfoliation and reassembly of HCN_3, adopted from our previous publication [41], is shown in Fig. 1. In a typical experiment, 54 mg of HCN_3 was placed into a tube with 50 mL of 0.004 M aqueous tetrabutylammonium hydroxide (TBAOH) and sonicated by a Hielscher UP200St (Germany) homogenizer (200 W) at half power for 5 min. After shaking at room temperature for 7 d, the mixture was sonicated for 5 min again. Hereafter bulk non-exfoliated particles were sedimented on a laboratory centrifuge ELMI CM-6MT (Latvia) at a separation factor F = 1000 for 1 h and the target suspension of the nanosheets was carefully separated from the precipitate with a pipette. The exfoliation experiments were repeated several times to obtain the required suspension volumes.

The reassembled niobate HCN_3 r/a was obtained via the vacuum filtration of the aforementioned suspensions on hydrophilic membrane Teflon filters with a pore size of 200 nm at a rate of 50 mL of the suspension per one filter. The target sample was rinsed with an excess of hot water, dried under ambient conditions and removed from the filters with a spatula.

Investigation of Photocatalytic Activity

Photocatalytic activity of the niobates obtained was studied in the reactions of hydrogen evolution from 1 mol % aqueous solutions of D-glucose and D-xylose under mid-near ultraviolet irradiation by DRT-125 (Russia) mercury lamp, 125 W, $\lambda > 220$ nm. The photocatalysts were tested both in an as-prepared state and after surface modification with a 1% Pt cocatalyst. The measurements were performed on the laboratory photocatalytic apparatus used in our previous publications [41–47] and included determination of the absolute ω and normalized per unit catalyst mass ω' rates of hydrogen generation, apparent quantum efficiency φ and the factor of increase in the reaction rate after platinization k_{Pt}. In each case, 25 mg of the photocatalyst was dispersed in 50 mL of aqueous glucose or xylose, loaded into the reaction cell and purged with argon to

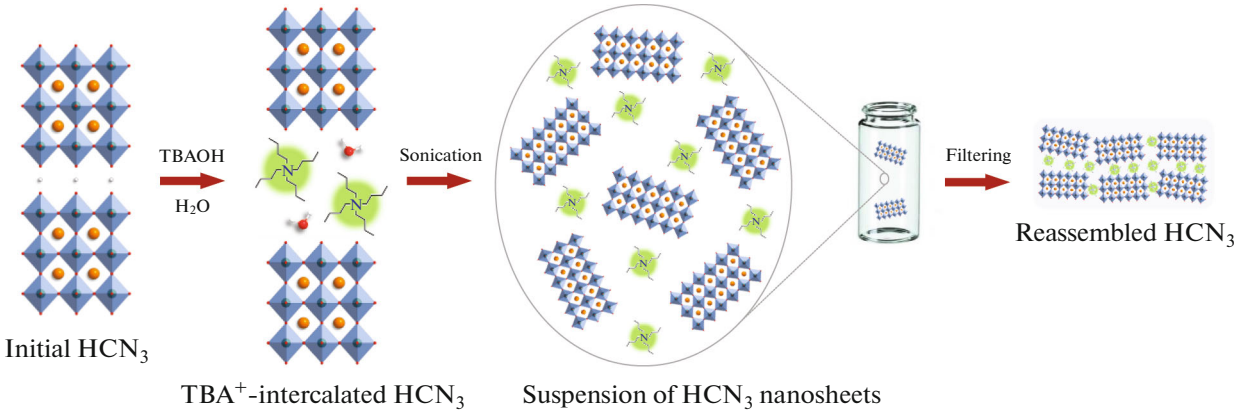

Fig. 1. Scheme for preparation of the reassembled niobate HCN_3 r/a.

remove residual air. When testing the activity with a Pt cocatalyst, 1 mL of a 1.28 mM H_2PtCl_6 aqueous solution was also injected into the suspension that was irradiated by a DRT-125 lamp to perform in situ photocatalytic platinization. After argon purging, the stirred reaction suspension was kept under irradiation for 2 h, during which the hydrogen content in the gas circuit was analyzed chromatographically at regular time intervals. After this, the light source was turned off to organize a dark stage and make sure that the photocatalytic reaction stops. For comparison, the similar experiments were conducted with a reference photocatalyst TiO_2 P25 Degussa. Finally, the areas of hydrogen chromatographic peaks were converted to hydrogen amounts that, in turn, were used to plot kinetic curves. The latter were approximated by linear functions and differentiated to find the hydrogen evolution rates ω. The apparent quantum efficiencies φ of the reactions were calculated using the equation

$$\varphi = 2\omega f^{-1} \times 100\%,$$

where f is the lamp photon flux in the photocatalyst absorption range measured previously via the conventional ferrioxalate actinometry method as described in open-access supporting materials to our previous publication [46].

Instrumentation and Data Processing

Powder X-ray diffraction (XRD) patterns of the samples were obtained on a Rigaku Miniflex II (Japan) benchtop Röntgen diffractometer (CuK_α radiation, angle range $2\theta = 3°–60°$, scanning rate 10°/min). Phase composition was controlled using Rigaku PDXL 2 software and powder diffraction files (PDF) of The International Centre for Diffraction Data (ICDD). Indexing of the diffraction patterns and calculation of the tetragonal lattice parameters were performed on the basis of all the reflections observed using DiffracPlus Topas software. Raman spectra were collected on a Bruker Senterra (Germany) spectrometer in the range of 50–4000 cm^{-1} using a 532 nm excitation laser (power–5 mW, accumulation time–30 s, 4 repetitions). Thermogravimetric (TG) analysis was carried out on a Netzsch TG 209 F1 Libra (Germany) thermobalance in a synthetic air atmosphere (temperature range 30–900°C, heating rate 10°C/min). Carbon and nitrogen content in the reassembled niobate was determined via the elemental CHN-analysis on a Euro EA3028-HT (Italy) analyzer. UV–Vis spectra of the samples dispersed in the carbohydrate solutions were recorded on a Thermo Scientific Genesys 10S UV-Vis (USA) spectrophotometer. Morphology of the samples was studied on a Zeiss Merlin (Germany) scanning electron microscope (SEM) equipped with a field emission cathode, electron optics column Gemini II and oil-free vacuum system. Specific surface area was measured on a Quadrasorb SI (USA) adsorption analyzer. Prior to analysis, 150–200 mg of each sample was degassed for 12 h without heating. Adsorption isotherms were measured at a liquid nitrogen temperature (−196°C) with nitrogen as an adsorptive. The values of specific surface area were calculated via the conventional multipoint Brunauer–Emmett–Teller (BET) method. Diffuse reflectance spectra (DRS) were recorded using a Shimadzu UV-2550 (Japan) spectrophotometer equipped with an ISR-2200 integrating sphere in the range of 220–800 nm with barium sulfate as a reference. The spectra obtained were transformed into coordinates $(Fh\nu)^{1/2} = f(h\nu)$, where $F = (1-R)^2/2R$ is the Kubelka–Munk function of a reflection coefficient R. Low-energy shoulders of the graphs were extrapolated to intersect the baseline and an abscissa of the intersection point was considered an optical bandgap energy E_g.

RESULTS AND DISCUSSION

Characterization of Initial and Reassembled HCN_3

The present study deals with two main objects: the initial protonated niobate HCN_3 and its reassembled

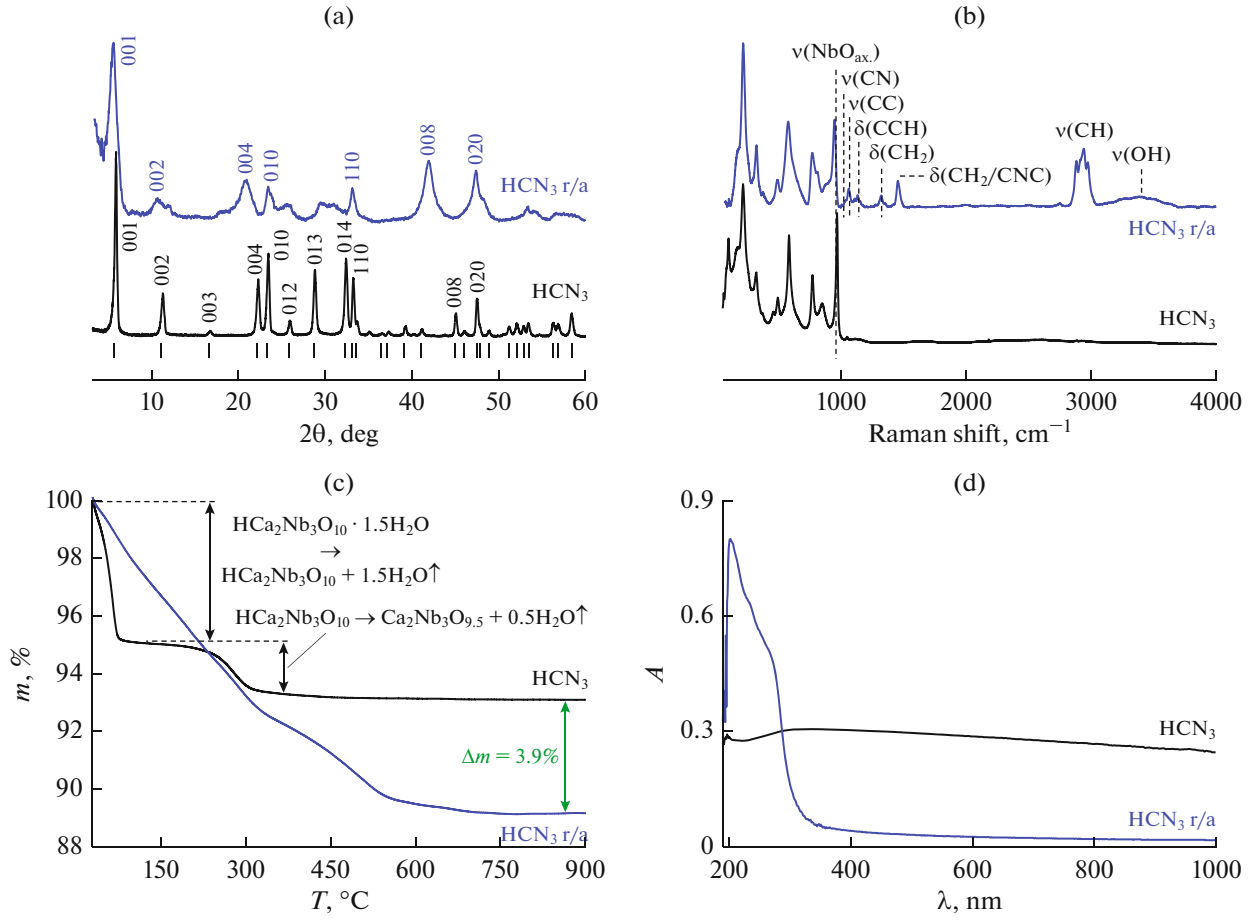

Fig. 2. XRD patterns (a), Raman spectra (b), TG curves (c) and UV–Vis spectra after dispersing in 1 mol % aqueous glucose (d) for the initial and reassembled niobates.

form HCN_3 r/a prepared via the liquid-phase exfoliation of the former into nanosheets and their restacking upon the filtration of the suspensions.

Primary characterization of the both samples was carried out using powder XRD analysis (Fig. 2a). It was established that HCN_3 was successfully synthesized in a single-phase state and its diffraction pattern is consistent with the PDF card no. 00-039-0915. All the reflections observed are amenable to indexing in the tetragonal system and the lattice parameters determined (Table 1) are in good consistency with the literarure data [27]. As can be seen from Fig. 2a, exfoliation and reassembly of the niobate lead to the formation of the layered phase with noticeably widened diffraction maxima, which, apparently, is associated with a pronounced disorder in stacking individual perovskite nanosheets upon the reassembly as well as a general decrease in particle sizes. That being said, positions of (010), (110) and (020) reflections as well as the *a* lattice parameter stay practically unchanged pointing to the preservation of the perovskite slab structure (Table 1). At the same time, the reassembled niobate demonstrates a low-angle shift of the (00x) diffraction maxima and, accordingly, the enlarged *c* parameter, corresponding to a greater distance between the adjacent perovskite slabs than in the initial compound.

Table 1. Characterization of the initial and reassembled niobates*

Sample	*a*, Å	*c*, Å	*S*, $m^2\ g^{-1}$	E_g, eV	λ_{max}, nm
HCN_3	3.82	16.0	7.6	3.50	354
HCN_3 r/a	≈3.8	≈17	18	3.42	363

* *a* and *c* are tetragonal lattice parameters; *S* is the specific surface areas; E_g is the optical bandgap energies; λ_{max} is the long-wave intrinsic absorption edges.

In accordance with the Raman spectra (Fig. 2b), one of key reasons for the increased interlayer distance of the reassembled niobate consists in the presence of strongly adsorbed residual tetrabutylammonium cations TBA^+ that probably prevent the adjacent nanosheets from tighter closing. Despite thorough rinsing with an excess of hot water, these cations still remain in the sample, which gives grounds, in a sense, to consider the latter as an inorganic-organic compos-

ite material. Exfoliation and reassembly also cause a decrease in the frequency of the axial Nb–O vibrational mode located in the terminal perovskite octahedra from ~966 to ~946 cm^{-1} that is most sensitive to the interlayer composition. At the same time, most of the other Nb–O vibrational modes (<800 cm^{-1}) remain unchanged, additionally confirming the preservation of the perovskite structure.

During thermolysis, the reassembled niobate demonstrates a 3.9% greater total mass loss than the initial protonated compound (Fig. 2c). Together with the results of elemental CHN-analysis, these data indicate that the reassembled sample also contains a perceptible amount of embedded water molecules. The quantitative composition estimated on the basis of TG and CHN data corresponds to the formula $H_{0.8}Ca_2Nb_3O_{10}\cdot 0.2TBA\cdot 0.75H_2O$. At the same time, the initial niobate contains twice as much intercalated water and its true composition should be presented in the form $HCa_2Nb_3O_{10}\cdot 1.5H_2O$. Moreover, the appearance of TG curves of the compounds in question is different (Fig. 2c). Particularly, the curve of the initial niobate includes two well-distinguishable steps corresponding to deintercalation of the interlayer water (30–150°C) and subsequent decomposition of the anhydrous protonated compound (275–450°C). The curve of the reassembled sample, on the contrary, exhibit gradual mass loss that is difficult to divide into individual stages. Such thermolysis kinetics, probably, is associated with the aforementioned disorder in stacking perovskite nanosheets appeared upon their reassembly.

Morphology and specific surface area of the samples were investigated using SEM and BET methods. As can be seen from Fig. 3, the initial protonated niobate consists of monolithic lamellar particles with predominant lateral dimensions of 500–1000 nm and a thickness of 150–300 nm. Its reassembled counterpart, on the contrary, is formed by distorted perovskite nanosheets with irregularly shaped edges that are stacked into aggregates of micrometer sizes. Specific surface area of the reassembled niobate, being equal to 18 $m^2\,g^{-1}$, is only 2.3 times greater than that of the initial sample (Table 1), which is probably caused by the strong nanosheet aggregation. However, the reassembled compound appears to undergo the ultrasound-assisted disaggregation much easier than the initial one, which follows from UV-vis spectra of the corresponding suspensions in aqueous glucose (Fig. 2d). Particularly, the suspension of the protonated niobate exhibits approximately constant optical density over the entire spectrophotometric range due to the pronounced Mie scattering by the relatively large particles. In the case of the reassembled sample, the suspension's spectrum shows intense bands of scattering and absorption only in the ultraviolet region while the optical density in the longer wavelength range tends to zero. These data indirectly indicate that sonication of the reassembled niobate in the glucose solution effectively disaggregates the stacked nanosheets and provides much smaller particle sizes in a dispersed state in comparison with those observed for the solid reassembled niobate (Figs. 3c, 3d).

The region of intrinsic light absorption of the photocatalysts under consideration was studied by means of DRS with the Kubelka–Munk transformation (Fig. 4). The exfoliation and reassembly resulted in a slight decrease in the optical bandgap energy from 3.50 to 3.42 eV corresponding to the bathochromic shift of the long-wave absorption edge from 354 to 363 nm (Table 1), which formally allows the reassembled photocatalyst to utilize a slightly wider radiation range. The observed band gap narrowing is apparently caused by an upward shift of the valence band maximum, formed predominantly by oxygen 2p-orbitals, during the transformation of the interlayer space into the external surface.

Photocatalytic Activity in the Reactions of Hydrogen Production

Photocatalytic performance of the niobates was tested in the reactions of hydrogen production from 1 mol % aqueous solutions of typical plant biomass components, glucose and xylose, under mid-near ultraviolet radiation ($\lambda > 220$ nm) of the 125 W mercury lamp. The kinetic curves obtained (Fig. 5) demonstrate linear behavior indicating the preservation of the stable reaction rate throughout the whole measurement time. When the lamp is turned off, all the curves reach a plateau corresponding to a zero activity in the dark mode.

It was found that even the initial niobate HCN_3 without additional modifications exhibits higher efficiency of hydrogen generation from aqueous glucose and xylose ($\varphi = 0.25$ and 0.21%, respectively) (Table 2) than the reference photocatalyst TiO_2 P25 Degussa tested under the same conditions ($\varphi \approx 0.15\%$) although the latter possesses much greater specific surface area (~50 $m^2\,g^{-1}$) in comparison with HCN_3 (7.6 $m^2\,g^{-1}$). Accordingly, the niobate's activity normalized per unit surface area formally proves to be approximately one order of magnitude greater that of TiO_2 P25 Degussa. This experimental fact once again indicates the advantage of the layered perovskite structure for photocatalytic applications over that of non-layered analogues. Further enhancement of the niobate's hydrogen evolution activity may be realized via its decoration with nanoparticles of a Pt cocatalyst that serve as active hydrogen formation sites, improve spatial charge separation and reduce the overpotential of this half-reaction [48]. In this case, the activity increases 6–7 times and apparent quantum efficiency φ reaches 1.5–1.6% (Table 2).

Exfoliation and reassembly of HCN_3 allowed significantly improving the efficiency of photocatalytic hydrogen production via glucose and xylose reforming. Particularly, HCN_3 r/a modified with 1% Pt was

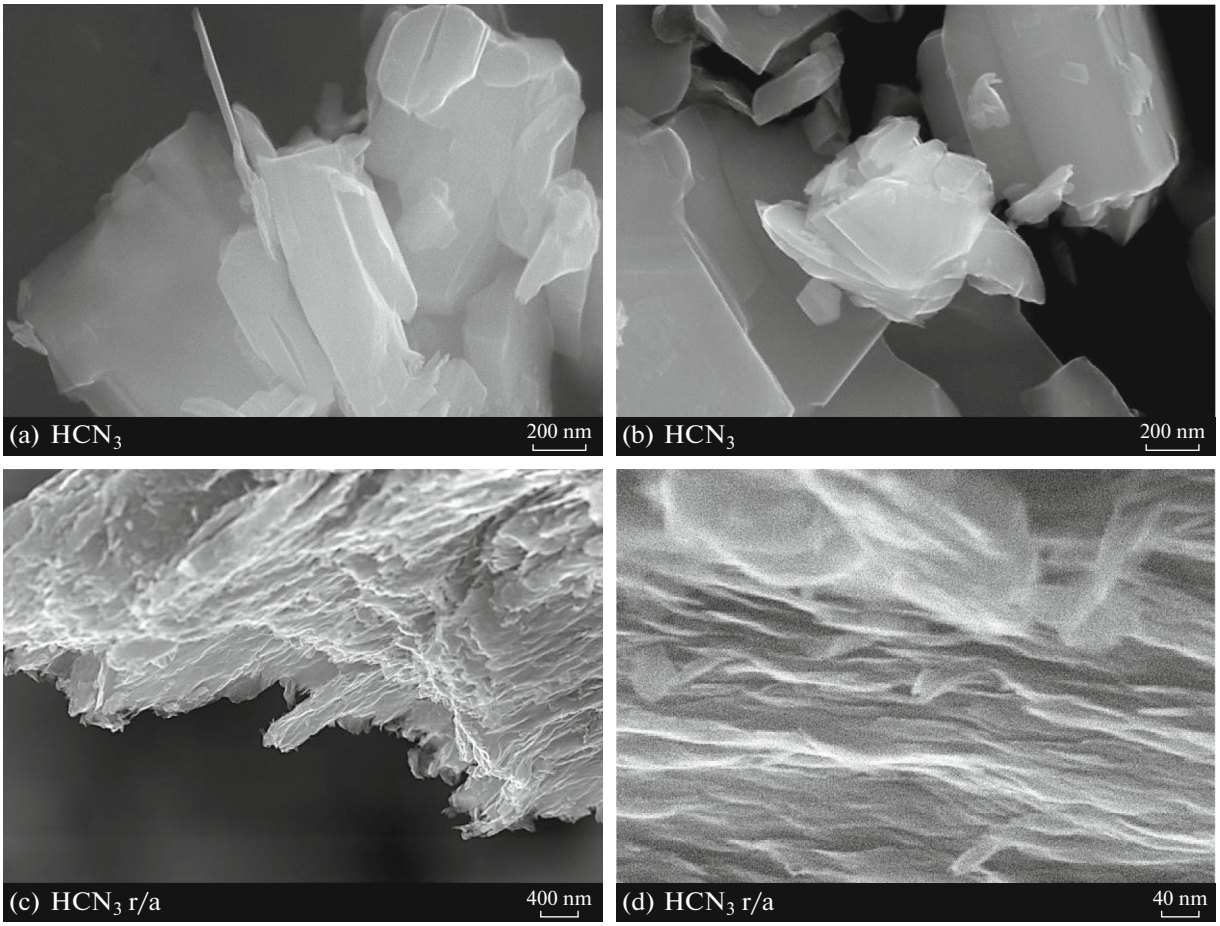

Fig. 3. SEM images of the initial (a, b) and reassembled (c, d) niobates.

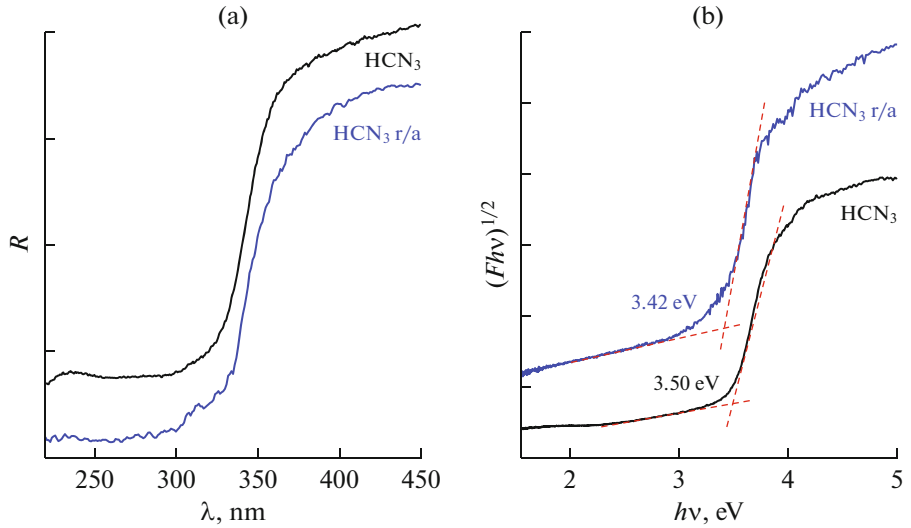

Fig. 4. Diffuse reflectance spectra (a) and corresponding Kubelka-Munk plots (b) for the initial and reassembled niobates.

shown to outperform the platinized HCN_3 by up to 6.3 times providing the activity of 24.2 mmol h^{-1} g^{-1} ($\varphi = 10\%$) and 22.8 mmol h^{-1} g^{-1} ($\varphi = 9.4\%$) in aqueous glucose and xylose, respectively (Table 2). Moreover, the quantum efficiencies achieved were revealed to be several times higher than those demonstrated by pla-

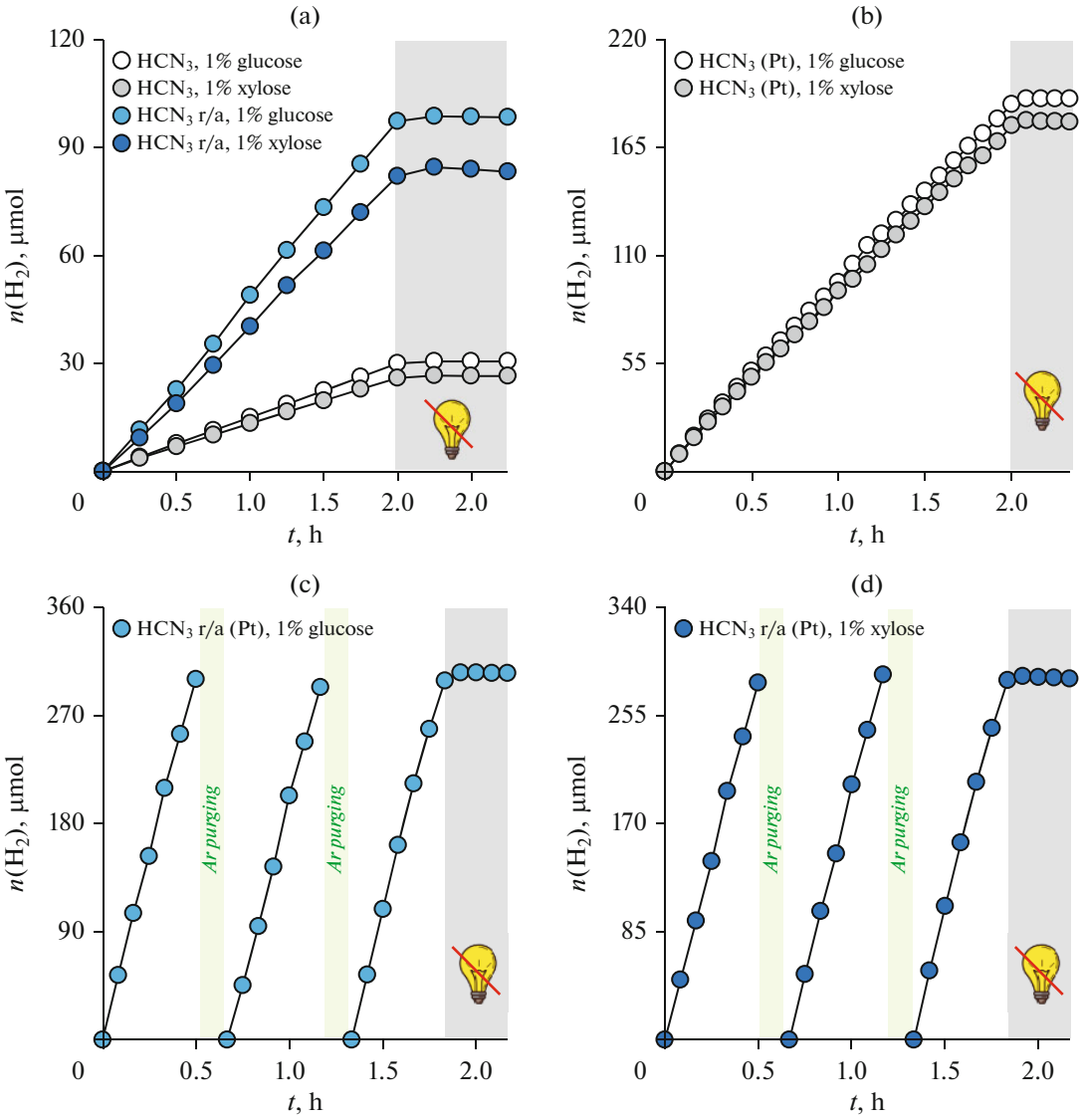

Fig. 5. Kinetic curves of photocatalytic hydrogen evolution from 1 mol % aqueous solutions of glucose and xylose over the initial and reassembled niobates in a bare state (a) and with a 1% Pt cocatalyst (b–d).

tinized TiO_2 P25 Degussa (Table 3) and slightly greater than measured for the organically modified HCN_3 (up to 8.8%) in one of our previous publications [39].

Figure 6 clearly compares the highest hydrogen evolution efficiencies achieved here over the platinized HCN_3 and HCN_3 r/a in the carbohydrates as well as those measured by our research team in pure water and aqueous methanol earlier with all other conditions being equal [41]. As one can see, the activity of HCN_3 decreases by 5 times when going from methanol to the carbohydrates. One of potential reasons for this consists in the limited steric accessibility of the HCN_3 interlayer rection zone for relatively large glucose and xylose molecules unlike methanol ones that are believed to penetrate this space and experience oxidation there. In the case of HCN_3 r/a, the photocatalytic reaction predominantly proceeds on the nanosheets' external surface, which removes the above steric limitations and the difference between the activity exhibited in the solutions of methanol and carbohydrates becomes significantly less pronounced (Fig. 6). Thus, the reassembled niobate nanosheets can serve as an efficient photocatalyst for hydrogen production from both methanol and carbohydrate aqueous solutions.

Table 3 summarizes the hydrogen evolution rates from glucose and xylose solutions achieved over the most promising photocatalysts reported over recent years. It is clearly seen that the reassembled niobate under consideration demonstrates a respectable activity level and, importantly, compares favorably with many composite photocatalysts in the ease of its preparation. However, different research teams use unequal condi-

Table 2. Photocatalytic activity of the initial and reassembled niobates in the reactions of hydrogen production from aqueous solutions of carbohydrates*

Solution	Photocatalyst	ω, μmol h^{-1}	ω', mmol h^{-1} g^{-1}	φ, %	k_{Pt}
1 mol % glucose	HCN_3	14.9	0.596	0.25	–
	HCN_3 (Pt)	95.8	3.83	1.6	6.4
	HCN_3 r/a	49.3	1.97	0.81	–
	HCN_3 r/a (Pt)	604	24.2	10	12
1 mol % xylose	HCN_3	12.9	0.516	0.21	–
	HCN_3 (Pt)	90.4	3.62	1.5	7.0
	HCN_3 r/a	41.5	1.66	0.69	–
	HCN_3 r/a (Pt)	570	22.8	9.4	14

* ω and ω' are the absolute and normalized per unit catalyst mass rates of hydrogen generation; φ is the apparent quantum efficiencies; k_{Pt} is the platinization efficiency coefficients.

Table 3. Comparison of hydrogen evolution rates in aqueous solutions of carbohydrates achieved over the reassembled niobate and TiO_2 P25 Degussa in this study as well as over most active photocatalysts reported in the latest publications

№	Photocatalyst	Solution	Irradiation	ω', mmol h^{-1} g^{-1}	Ref.
1	HCN_3 r/a, 1% Pt	Glucose 1 mol %	125 W Hg lamp, λ > 220 nm	24.2	This study
2		Xylose 1 mol %		22.8	
3	TiO_2 P25 Degussa, 1% Pt	Glucose 1 mol %	125 W Hg lamp, λ > 220 nm	8.89	This study
4		Xylose 1 mol %		11.8	
5	CdS/MoS_2	Glucose 0.1 M	300 W Xe lamp, λ > 400 nm	55	[49]
6	$Cd_{0.6}Zn_{0.4}S/Cd_{0.1}Zn_{0.9}S$, 1% Pt	Glucose 0.045 M	LED 450 nm, 48 mW cm^{-2}	3.4	[50]
7		Xylose 0.015 M		1.0	
8	g-C_3N_4, 2% Pt-Au	Glucose 0.16 M	300 W Xe lamp, λ = 350–800 nm, 170 mW cm^{-2}	2.37	[51]
9	$CaTiO_3/Zn_{0.3}Cd_{0.7}S$	Glucose 0.1 M	300 W Xe lamp	2.81	[52]
10	$LaFeO_3$, 0.7% Rh	Glucose 1 g L^{-1}	10 W LED, λ = 375–380 nm	1.84	[53]
11	TiO_2-$W_{0.25}$, Pt	Glucose 0.001 M	150 W halogen lamp	0.12	[54]
12	g-C_3N_4 oxidized, 3% Pt	Glucose 1 M	Simulated solar light, 500 W m^{-2}	0.87	[55]
13	$Zn_{0.6}Cd_{0.4}S$	Glucose 20 g L^{-1}	300 W Xe lamp	0.69	[56]
14	$Mn_{0.7}Cd_{0.3}S$	Xylose 2 g L^{-1}	300 W Xe lamp	14.1	[57]

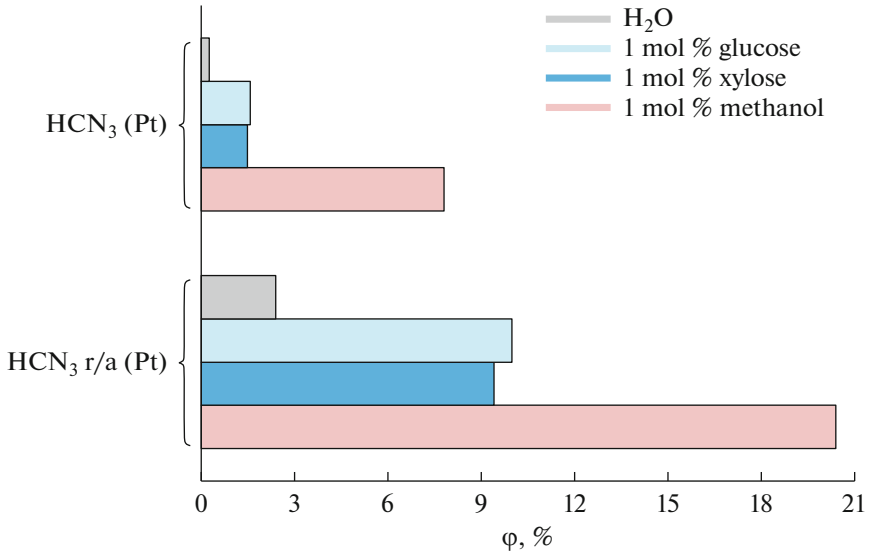

Fig. 6. Apparent quantum efficiency φ of photocatalytic hydrogen evolution over the initial and reassembled niobates with a 1% Pt cocatalyst from pure water as well as 1 mol % aqueous solutions of glucose, xylose and methanol.

tions of photocatalytic measurements, and a strict comparison of the results of this study with those presented in the literature does not seem entirely possible.

CONCLUSIONS

In this study, the layered perovskite-structured niobate $HCa_2Nb_3O_{10}$ has been exfoliated into nanosheets and reassembled to yield an efficient photocatalyst for hydrogen generation from typical biomass components—glucose and xylose. Thanks to the increased specific surface area and improved dispersibility, the reassembled niobate outperformed in the activity the initial compound and reference photocatalyst TiO_2 P25 Degussa by up to 6.3 and 5.3 times, respectively, providing a hydrogen production rate up to 24.2 mmol $h^{-1}g^{-1}$ and apparent quantum efficiency up to 10% in the mid-near ultraviolet range.

ACKNOWLEDGMENTS

The research was conducted using the equipment of the Saint Petersburg State University Research Park: Center for X-ray Diffraction Studies, Center for Optical and Laser Research, Center for Chemical Analysis and Materials Research, Center for Thermal Analysis and Calorimetry, Interdisciplinary Center for Nanotechnology, Center for Diagnostics of Functional Materials for Medicine, Pharmacology and Nanoelectronics.

FUNDING

The research was supported by the Russian Science Foundation (grant no. 22-73-10110).

CONFLICT OF INTEREST

The authors of this work declare that they have no conflicts of interest.

REFERENCES

1. Christoforidis, K.C. and Fornasiero, P., *ChemCatChem,* 2017, vol. 9, no. 9, p. 1523.
2. Puga, A.V., *Coord. Chem. Rev.,* 2016, vol. 315, p. 1.
3. Ramis, G., Bahadori, E., and Rossetti, I., *Int. J. Hydrogen Energy,* 2020, vol. 46, no. 22, p. 12105.
4. Davis, K.A., Yoo, S., Shuler, E.W., Sherman, B.D., Lee, S., and Leem G., *Nano Converg.,* 2021, vol. 8, p. 6.
5. Kuehnel, M.F. and Reisner, E., *Angew. Chem. Int. Ed.,* 2018, vol. 57, no. 13, p. 3290.
6. Jaswal, R., Shende, R., Nan, W., and Shende, A., *Int. J. Hydrogen Energy,* 2017, vol. 42, no. 5, p. 2839.
7. Sun, Z., Zhao, H., Yu, X., Hu, J., and Chen, Z., *Chem. Synth.,* 2024, vol. 4, p. 4.
8. Skvortsova, L.N., Artyukh, I.A., Tatarinova, T.V., and Bolgaru, K.A., *Kinet. Catal.,* 2024, vol. 65, no. 2, p. 101.
9. Markovskaya, D.V. and Kozlova, E.A. *Kinet. Catal.,* 2018, vol. 59, no. 6, p. 727.
10. Roongraung, K., Cherevan, A., Eder, D., and Chuangchote, S., *Catal. Sci. Technol.,* 2023, vol. 13, no. 19, p. 5556.

11. Kharina, S.N., Kurenkova, A.Yu., Saraev, A.A., Gerasimov, E.Yu., and Kozlova, E.A., *Nanosyst. Phys. Chem. Math.,* 2024, vol. 15, no. 3, p. 388.
12. Mu, Z., Zou, R., Yang, W., Ma, J., Chen, Z., Shi, G., Liu, J., Li, T., Liu, Y., and Peng X., *ACS Sustain. Chem. Eng.,* 2023, vol. 11, no. 28, p. 10233.
13. Bie, C., Wang, L., and Yu, J., *Chem. Cell Press,* 2022, vol. 8, no. 6, p. 1567.
14. Gupta, A., Likozar, B., Jana, R., Chanu, W.C., and Singh, M.K., *Int. J. Hydrogen Energy,* 2022, vol. 47, no. 78, p. 33282.
15. Hota, P., Das, A. and Maiti, D.K., *Int. J. Hydrogen Energy,* 2023, vol. 48, no. 2, p. 523.
16. Vorontsov, A.V., Kozlova, E.A., Besov, A.S., Kozlov, D.V., Kiselev, S.A., and Safatov, A.S., *Kinet. Catal.,* 2010, vol. 51, no. 6, p. 801.
17. Bellardita, M., García-López, E., Marcì, G., and Palmisano, L., *Int. J. Hydrogen Energy,* 2016, vol. 41, no. 14, p. 5934.
18. Zhou, M., Li, Y., Peng, S., Lu, G., and Li, S., *Catal. Commun.,* 2012, vol. 18, p. 21.
19. Bahadori, E., Ramis, G., Zanardo, D., Menegazzo, F., Signoretto, M., Gazzoli, D., Pietrogiacomi, D., Michele, A.D., and Rossetti, I., *Catalysts,* 2020, vol. 10, no. 5, p. 477.
20. Iervolino, G., Vaiano, V., Murcia, J.J., Rizzo, L., Ventre, G., Pepe, G., Campiglia, P., Hidalgo, M.C., Navío, J.A., and Sannino, D., *J. Catal.,* 2016, vol. 339, p. 47.
21. Bello, M.O., Shelake, S.P., Abdus-Salam, N., Adekola, F.A., Vennapoosa, C.S., Sainath, A.V.S., and Pal, U., *Catal. Commun.,* 2024, vol. 186, p. 106817.
22. Fujishima, A. and Honda, K., *Nature,* 1972, vol. 238, no. 5358, p. 37.
23. Irshad, M., Aina, Q., Zamana, V., Aslama, M.A., Kousara, N., Asima, M., Rafique, M., Siraja, K., Tabishc, A.N., Usmand, M., Farooqe, M.H., Assirif, M.A., and Imran, M., *RSC Adv.,* 2022, vol. 12, no. 12, p. 7009.
24. Rodionov, I.A. and Zvereva, I.A., *Russ. Chem. Rev.,* 2016, vol. 85, no. 3, p. 248.
25. Maeda, K. and Mallouk, T.E., *Bull. Chem. Soc. Jpn.,* 2018, vol. 92, no. 1, p. 38.
26. Hu, Y., Mao, L., Guan, X., Tucker, K.A., Xie, H., Wu, X., and Shi, J., *Renewable Sustainable Energy Rev.,* 2020, vol. 119, p. 109527.
27. Jacobson, A.J., Lewandowski, J.T., and Johnson J.W., *J. Less Common Met.,* 1986, vol. 116, no. 1, p. 137.
28. Ebina, Y., Sasaki, T., Harada, M., and Watanabe M., *Chem. Mater.,* 2002, vol. 1, no. 12, p. 4390.
29. Maeda, K. and Mallouk, T.E., *J. Mater. Chem.,* 2009, vol. 19, no. 27, p. 4813.
30. Shi, J., Mao, L., Cai, C., Li, G., Cheng, C., Zheng, B., Hu, Y., Huang, Z., Hue, X., and Żyła, G., *Catal. Sci. Technol.,* 2020, vol. 10, no. 17, p. 5896.
31. Xiong, J., Jing, K., Zou, J., Liang, S., and Wu, L., *Dalton Trans.,* 2017, vol. 46, no. 40, p. 13935.
32. Hu, Y., Li, G., Zong, S., Shi, J., and Guo, L., *Catal. Today,* 2018, vol. 315, p. 117.
33. Xie, Z., Liang, X., Jiang, D., and Chen, M., *Nanotechnology,* 2020, vol. 31, no. 32, p. 325401.
34. Li, D., Zhou, C., Liang, X., Shi, X., Song, Q., Chen, M., and Jiang, D., *Colloids Surf. A: Physicochem. Eng. Asp.,* 2021, vol. 615, p. 126252.
35. Li, D., Zhao, H., Li, L., Mao, B., Chen, M., Shen, H., Shi, W., Jiang, D., and Lei, Y., *Adv. Funct. Mater.,* 2018, vol. 28, no. 52, p. 1806284.
36. Nishioka, S., Oshima, T., Hirai, S., Saito, D., Hojo, K., Mallouk, T.E., and Maeda, K., *ACS Catal.,* 2021, vol. 11, no. 2, p. 659.
37. Maeda, K., Sahara, G., Eguchi, M., and Ishitani, O., *ACS Catal.,* 2015, vol. 5, no. 3, p. 1700.
38. Greene, W.N. and Roy, N., *J. Phys. Chem. C.,* 2009, vol. 113, no. 18, p. 7962.
39. Kurnosenko, S.A., Voytovich, V.V., Silyukov, O.I., Rodionov, I.A., and Zvereva, I.A., *Nanomaterials,* 2022, vol. 12(15), p. 2717.
40. Tahara, S. and Sugahara, Y., *Langmuir,* 2003, vol. 19, no. 22, p. 9473.
41. Kurnosenko, S.A., Voytovich, V.V., Silyukov, O.I., Rodionov, I.A., Malygina, E.N., and Zvereva, I.A, *Catalysts,* 2023, vol. 13, no. 3, p. 614.
42. Rodionov, I.A., Maksimova, E.A., Pozhidaev, A.Y., Kurnosenko, S.A., Silyukov, O.I., and Zvereva, I.A., *Front. Chem.,* 2019, vol. 7, p. 863.
43. Rodionov, I.A., Gruzdeva, E.O., Mazur, A.S., Kurnosenko, S.A., Silyukov, O.I., and Zvereva, I.A., *Catalysts*, 2022, vol. 12, no. 12, p. 1556.
44. Voytovich, V.V., Kurnosenko, S.A., Silyukov, O.I., Rodionov, I.A., Minich, I.A., and Zvereva, I.A., *Front. Chem.*, 2020, vol. 8, p. 300.
45. Voytovich, V.V., Kurnosenko, S.A., Silyukov, O.I., Rodionov, I.A., Bugrov, A.N., Minich, I.A., Malygina, E.N., and Zvereva, I.A., *Catalysts,* 2021, vol. 11, no. 8, p. 897.
46. Kurnosenko, S.A., Voytovich, V.V., Silyukov, O.I., Rodionov, I.A., and Zvereva, I.A, *Catalysts,* 2023, vol. 13, no. 4, p. 749.
47. Kurnosenko, S.A., Voytovich, V.V., Silyukov, O.I., Rodionov, I.A., Kirichenko, S.O., Minich, I.A., Malygina, E.N., Khramova, A.D., and Zvereva, I.A., *Catalysts,* 2021, vol. 11, no. 11, p. 1279.
48. Al-Azri, Z.H.N., Chen, W-T., Chan, A., Jovic, V., In, T., Idriss, H., and Waterhouse, G.I.N., *J. Catal.,* 2015, vol. 329, p. 355.
49. Li, C., Wang, H., Ming, J., Liu, M., and Fang, P., *Int. J. Hydrogen Energy,* 2017, vol. 42, no. 27, p. 16968.
50. Kurenkova, A.Y., Markovskaya, D.V., Gerasimov, E.Y., Prosvirin, I. P., Cherepanova, S.V., and Kozlova, E.A., *Int. J. Hydrogen Energy,* 2020, vol. 45, no. 55, p. 30165.

51. Ding, F., Yu, H., Liu, W., Zeng, X., Li, S., Chen, L., Li, B., Guo, J., and Wu, C., *Mater. Des.,* 2024, vol. 238, p. 112678.

52. Bai, F.Y., Han, J.R., Chen, J., Yuan, Y., Wei, K., Shen, Y.S., Huang, Y.F., Zhao, H., Liu, J., Hu, Z.Y., Li, Y., and Su, B.L., *J. Colloid Interface Sci.,* 2023, vol. 638, p. 173.

53. Vaiano, V., Iervolino, G., Sannino, D., *Chem. Eng. Trans.,* 2017, vol. 60, p. 235.

54. Bellardita, M., García-López, E.I., Marcì, G., Nasillo, G., and Palmisano, L., *Eur. J. Inorg. Chem.,* 2018, vol. 2018, no. 41, p. 4522.

55. Speltini, A., Scalabrini, A., Maraschi, F., Sturini, M., Pisanu, A., Malavasi, L., and Profumo, A., *Int. J. Hydrogen Energy,* 2018, vol. 43, no. 32, p. 14925.

56. Zhao, H., Li, C.F., Yong, X., Kumar, P., Palma, B., Hu, Z.Y., Van Tendeloo, G., Siahrostami, S., Larter, S., Zheng, D., Wang, S., Chen, Z., Kibria, M.G., and Hu, J., *Science,* 2021, vol. 24, no. 2, p. 102109.

57. Liu, Y., Kang, F., Bi, C., Shi, J., Gao, G., An, Y., and Huang, Z., *J. Colloid Interface Sci.,* 2023, vol. 652, p. 2066.